



Article

# Hybrid Fabrication of Zirconia Parts with Smooth Surface Texture and Tight Tolerances

Laurent Spitaels <sup>1</sup>, Valentin Dambly <sup>1</sup>, Aiora Beobide Otaegi <sup>2</sup>, Julien Bossu <sup>1</sup>, Cathy Delmotte <sup>3</sup>, Gregory Martic <sup>3</sup>, Enrique Juste <sup>3</sup>, Raoul Carrus <sup>4</sup>, Pedro-José Arrazola <sup>2</sup>, Fabrice Petit <sup>3</sup>, Edouard Rivière-Lorphèvre <sup>1</sup> and François Ducobu <sup>1,\*</sup>

<sup>1</sup> UMONS Research Institute for Materials Science and Engineering, University of Mons, Place du Parc 20, 7000 Mons, Belgium

<sup>2</sup> Faculty of Engineering, Mondragon Unibertsitatea, Loramendi 4, 20500 Arrasate-Mondragón, Spain

<sup>3</sup> Belgium Ceramic Research Centre, Avenue Gouverneur Cornez 4, 7000 Mons, Belgium

<sup>4</sup> SIRRIIS, Collective Centre for and by the Technological Industry, 12 Rue Bois Saint Jean, 4102 Seraing, Belgium

\* Correspondence: francois.ducobu@umons.ac.be

**Abstract:** The conventional manufacturing chain for technical ceramics is too expensive for the production of small series or unique parts with complex designs. Hybrid machines that combine additive and subtractive processes can be an interesting solution to overcome this technology lock-in. However, despite the great interest in hybrid machines for metallic parts, there is a lack of data in the literature when it comes to ceramics. The purpose of this paper is to contribute to closing this gap. It is the first to evaluate the achievable geometrical tolerances according to ISO 2768-2 as well as the surface textures of composite zirconia parts shaped sequentially by pellet additive manufacturing (PAM, from ceramic injection molding feedstock) and finish milling. The green parts were then debinded and sintered to analyze the influence of these steps. Compared to the initial green parts, the sintered parts exhibited shiny and smooth surfaces with sharp edges. Flatness, parallelism and perpendicularity all achieved an H (fine) class, while the surface textures were significantly improved, resulting in arithmetic roughness (Ra) below 1.6  $\mu\text{m}$ .

**Keywords:** material extrusion; surface texture; geometrical tolerances; zirconia; milling; hybrid; composite



**Citation:** Spitaels, L.; Dambly, V.; Beobide Otaegi, A.; Bossu, J.; Delmotte, C.; Martic, G.; Juste, E.; Carrus, R.; Arrazola, P.-J.; Petit F.; et al. Hybrid Fabrication of Zirconia Parts with Smooth Surface Texture and Tight Tolerances. *J. Compos. Sci.* **2024**, *8*, 233. <https://doi.org/10.3390/jcs8070233>

Academic Editor: Chensong Dong

Received: 8 May 2024

Revised: 6 June 2024

Accepted: 20 June 2024

Published: 22 June 2024



**Copyright:** © 2024 by the authors. Licensee MDPI, Basel, Switzerland. This article is an open access article distributed under the terms and conditions of the Creative Commons Attribution (CC BY) license (<https://creativecommons.org/licenses/by/4.0/>).

## 1. Introduction

Technical ceramics such as zirconium oxides ( $\text{ZrO}_2$ ) and its derivatives (such as 3Y-TZP, for example) find applications in diverse industries (mechanical, chemical, biomedical and electrical) [1,2]. The fracture toughness and flexural strength of such materials are among the highest available for ceramics, with ranges of 4–12  $\text{MPa}\sqrt{\text{m}}$  and 500–1800 MPa, respectively [3]. The other advantages of technical ceramics compared to conventional materials such as metals are their higher melting point, higher hardness, excellent corrosion resistance and lower thermal conductivity [2].

However, the conventional manufacturing chain followed to shape parts in technical ceramics is not capable of realizing small batches or unique parts without prohibitive cost [2]. Yet such a low quantity of parts is mandatory, especially for the production of customized implants, where each patient is unique and requires a specific design [4]. The usual route followed to manufacture parts in ceramics is composed of four main steps: feedstock preparation, shaping (e.g., by slip casting, extrusion, cold or hot isostatic pressing or ceramic injection molding (CIM)), debinding (chemical and/or thermal) and sintering [2]. Even though this process has been well known for decades, the tolerances and surface textures obtained after the sintering operation do not always comply with the final application of the parts. When it comes to finishing the parts and bringing them to the desired tolerances and surface textures, polishing, lapping or milling can be used [3]. Among these possibilities, the milling process is the most accurate and reliable way to

obtain the desired surface textures and geometries for complex parts [5]. Nevertheless, after sintering, the part acquires its final mechanical properties and exhibits very high hardness and strength. Therefore, the finish milling process requires expensive tools, which can represent up to 80% of the total manufacturing cost [3], and can lead to macro defects (such as cracks, for example) [5]. Trying to decrease the operations cost and improve the surface integrity is, therefore, essential.

Newly emerging processes such as additive manufacturing (AM) offer an interesting outcome for producing small batches or even unique parts with complex designs (e.g., functional tools, spare parts, prototypes, parts with non-conventional forms, jewels, etc.) without the need for expensive equipment dedicated to a single part design, such as mold, for example [2,6]. This is especially true for healthcare applications, which require parts with a personalized design dedicated to a single patient and exhibiting a complex geometry with controlled porosity and an intricate internal structure [7,8]. Among the seven families of AM processes defined by ISO 52900 [9], material extrusion (MEX) is seen as very promising [10]. This technology enables the shaping of green composite parts made of almost any type of ceramic material (oxide and non-oxide) at a 40% lower cost than the conventional route [11,12]. Variations exist among MEX printers depending on the composite feedstock used to manufacture the part: it can be filaments, pastes or even pellets [13–15]. Pastes and filaments suffer from lower availability compared to pellets [15]. Moreover, filaments are brittle at ambient temperature due to their loading, and they are costly to produce since their diameter variations should be within tight tolerances (<2% to ensure consistent flow rates) [13]. These reasons lead to higher prices and push the use of pellets. Indeed, these feedstocks have been used since the 1970s in the CIM industry [16] and present many advantages such as lower price, higher availability, lower brittleness and no preheating required [14,17]. The ceramic content of such composite feedstock can reach up to 60%vol [12]. The process that relies on machines fitted with an extrusion screw and uses pellets is called PAM (pellet additive manufacturing). This has been successfully tested using ceramic composite feedstock as described in the following references: [6,15,18,19].

However, despite the capabilities of PAM printers, the parts they produce still suffer from the common drawbacks of AM compared to conventional processes: slower production rates, higher specific energy consumption, rougher surface textures due to the staircase effect, and larger geometrical and dimensional tolerances [20–23]. Therefore, finishing the parts is still required. Machining, and especially milling, is able to achieve tight tolerances (IT7 from ISO 286-1) as well as smooth surface finishes ( $R_a < 0.4 \mu\text{m}$ ) [24]. When it is performed just after the shaping process, it is called green machining [3]. The part at the green state exhibits mainly pseudo-plastic behavior, which eases its finishing with resulting lower cutting forces, temperatures, induced residual stresses, energy consumption and tool wear [25]. All these advantages allow higher material removal rates and a reduction of the costs to be achieved [26,27]. Nevertheless, if finish milling is performed after the complete fabrication of the part, some of the part's areas will not be accessible to the milling tool [28].

This motivates the integration of the milling tool and spindle directly in the AM printer to obtain a hybrid machine that combines the additive and subtractive processes [28,29]. This architecture enables the surfaces to be finished progressively when they are still reachable and the production of parts with the same characteristics as those finished by milling during the green state [12]. Moreover, hybrid machines allow larger nozzle diameters to be selected since the imperfections of the printing process will be corrected by the milling operation [11]. The larger the nozzle diameter, the higher the productivity, since only a near-net-shape part has to be produced [29].

Despite a lot of interest in the production of hybrid machines to produce metallic parts [30], development concerning ceramics is still limited. There is a lack of data in the literature about the surface textures that can be achieved as well as the geometrical tolerances for these materials [11]. Moreover, the influence of the debinding and sintering processes following hybrid shaping operation is not well covered. This article therefore

aims to conduct tests to evaluate their influence and confirm if the acquired surface textures and geometrical tolerances can be maintained after the debinding and sintering operations.

Dedicated standards for the dimensional and geometrical tolerances as well as the textures of surfaces generated by AM are not yet available. For conventional processes, the dimensional tolerances can be set using ISO 286-1 [31] and ISO 2768-1 [32], the geometrical tolerances can be selected using ISO 2768-2 [33] and, finally, the surface texture indicators and measurements can be conducted following ISO 4288 [34]. According to the recent ISO 17296-3 [35], all these standards can be used for thermoplastic, metallic and ceramic parts shaped by AM since no dedicated AM standard exists for these purposes.

Therefore, this article is the first to:

- Quantify the improvements in surface texture and geometrical tolerances achieved by finish milling on green composite zirconia parts shaped by PAM according to ISO 4288 and ISO 2768-2;
- Evaluate the influence of the debinding and sintering operations on the achieved surface texture and geometrical tolerances;
- Assess the global improvements achievable in the entire hybrid manufacturing chain.

## 2. Materials and Methods

### 2.1. Composite Feedstock

The selected feedstock for the PAM process was Inmaflow K2015 from the Inmatec company (Rheinbach, Germany). These composite pellets exhibit a weight composition of 85wt% of zirconia powder ( $ZrO_2$  94.5%,  $Y_2O_3$ -partially stabilized, TZ-black from Tosoh Corp., Tokyo, Japan) and 15wt% thermoplastic binder (polyamide). The shrink factor announced by the pellet manufacturer is 1.280.

### 2.2. Global Experimental Steps and Part Design

The suitability of the hybrid approach was evaluated by following several experimental steps: the manufacturing of the parts by the PAM process, their finishing by milling operations, and their debinding and sintering. Since the foreseen hybrid machine is not yet available, the experiments were conducted with a sequential hybrid approach: the parts were first printed and then finished in a CNC machine. Each produced part was characterized dimensionally and geometrically, while its surface texture was also evaluated. These characterizations took place after the manufacturing by PAM, finish milling and sintering steps as shown in Figure 1. The parts did not have sufficient mechanical resistance to be characterized after the debinding process with devices such as a coordinate measuring machine (CMM), which relies on tactile probing. All the measurements allowed us to evaluate the state of the parts after their manufacturing and then to quantify the improvements brought by the milling operation. The final characterizations allowed us to assess if the debinding and sintering operations had a significant influence on the geometrical tolerances and surface textures obtained after the finish milling step.

The chosen part design was composed of a cube on top of a cylinder, as depicted in Figure 2. The top of the cube will be referred as the “Top” surface in the rest of the paper, while the side surfaces will be referred to as “Vertical” surfaces. The cube exhibited an edge dimension of 20 mm, while the cylinder had both a diameter and height of 15 mm. Finish milling operations were conducted on the cubic part; the cylinder was used to clamp the part into a three-jaw chuck. A 3 mm fillet linked the cube and the cylinder to avoid a brutal change in the section and stress concentrations [36]. As can be seen in Figure 1, the orientation of the part was modified for the milling operation (cube on top, cylinder below). On the other hand, the printing, debinding and sintering operations were all performed with the parts placed on their top surface (cube below, cylinder on top). This geometry of parts has been successfully used by previous studies that also machined green composite parts made of ceramic and thermoplastic shaped by PAM and finished by milling operations [27,37].

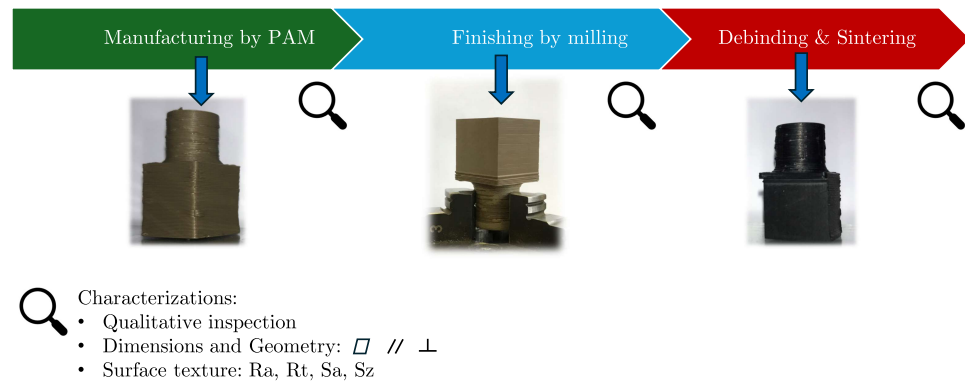


**Figure 1.** The three experimental steps performed as well as the manufactured part’s characteristics.

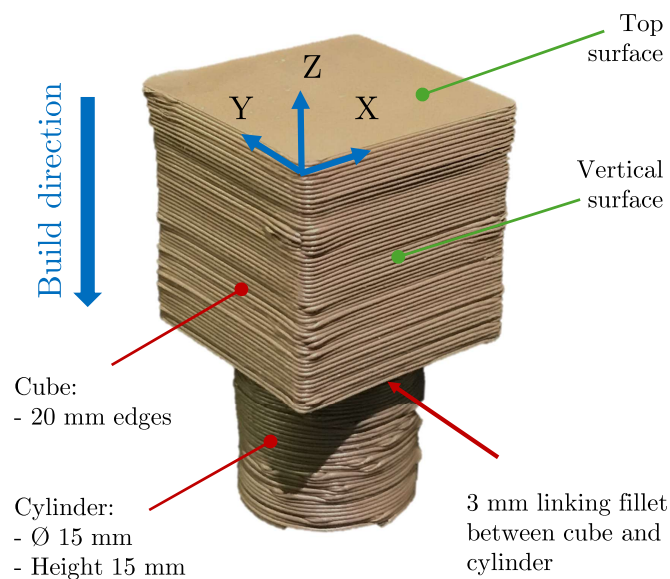


**Figure 2.** Selected part design.

**2.3. Step 1: Printing**

Three parts were printed by PAM using a Pollen AM Series MC printer (Ivry-sur-Seine, France). The nozzle diameter was 1 mm, ensuring fast production time for the parts (25 min per part). First, the cube was printed, and then the cylinder was printed. This allowed us to produce the parts without the need for a support structure. Therefore, the Top surface of the cube was in contact with the build platform of the printer. The other relevant printing parameters are given in Table 1. The software SolidWorks 2023 as well as Cura 4.13 were used to prepare the CAD model and the gcode, respectively. The file format for both software programs was STL.

**Table 1.** Printing parameters selected to manufacture the parts.

Nozzle diameter	1 mm
Layer thickness	0.350 mm
First layer thickness	0.170 mm
Extrusion temperature	165 °C
Build platform temperature	35 °C
Infill strategy	Concentric
Infill percentage	100%
Printing time	25 min/part

#### 2.4. Step 2: Finish Milling Operations

The parts were finished by dry milling operations outside of the PAM printer using a Stäubli TX-200 robotic arm (Pfäffikon, Switzerland) equipped with a Teknomotor ATC71 electrospindle (Quero, Italy). The spindle can reach a rotational speed of 24,000 rpm and can deliver up to 7.8 kW. The solid end-milling tool used had the reference 209425-6 and was supplied by Hoffmann. It exhibited three teeth and a 6 mm diameter. The selected cutting speed  $v_c$  was 339 m/min ( $N = 18,000$  rpm), while the feed rate was 1458 mm/min. These tool and cutting conditions were chosen according to a recent study on finishing green zirconia parts by milling operations [27].

The Top surface of the cube as well as three of the Vertical surfaces were machined. The fourth was kept as an “as-built” reference surface. As depicted in Figure 3, each plane of the part’s cubic section was given a name. The vertical surfaces were named “V1” to “V4”, while the top surface was named “Top”. These names will be used in the rest of the paper.

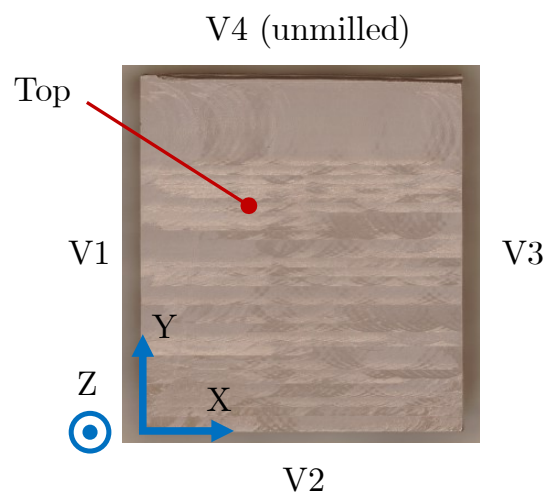


**Figure 3.** Names of the characterized surfaces and top view of a part; magnification 40×.

The thickness of material to be removed from the parts was selected depending on the as-built parts’ surface texture. This allowed the radial and axial depths of cut,  $a_e$  and  $a_p$ , respectively, to be determined. Preliminary measurements were conducted to determine the  $S_z$  (maximal height) indicator with the same configuration and parameter choice as the part characterization. For the sake of simplicity, the parameters used to conduct these first measurements are not repeated here and can be found in Section 2.6. The as-built parts exhibited a maximal  $S_z$  value of 125  $\mu\text{m}$  for the top surface, while it was up to 1467  $\mu\text{m}$  for the vertical surfaces. Therefore, the chosen thickness to be removed was 0.2 mm and 1.5 mm for the Top and Vertical surfaces, respectively. Since the Top surface is machined using end milling (following the X-axis direction), the chosen radial and axial depths of cut,  $a_e$  and  $a_p$ , were 0.5 mm and 0.2 mm, respectively. By contrast, each Vertical surface was machined using side milling with three passes at  $a_e = 0.5$  mm and  $a_p = 3$  mm. The cutting parameters are summed up in Figure 4. All the operations were conducted using conventional dry milling.

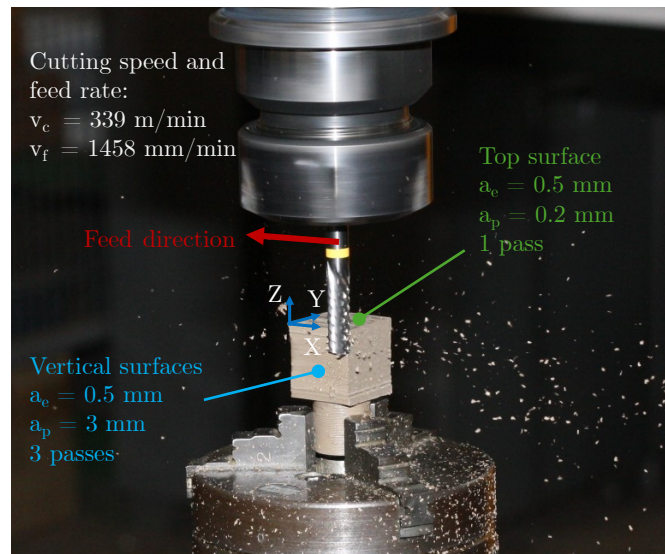


**Figure 4.** The parameters and configuration of the milling operation—finishing of a Vertical surface.

### 2.5. Step 3: Debinding and Sintering Operations

During the debinding and sintering operations, the parts were placed on their Top surface. Following the recommendations of the pellet supplier, debinding was performed in two steps. The first consisted of chemical debinding by immersing the parts in an acetone bath at 45 °C. This step was followed by thermal debinding with a plateau reaching 300 °C. Thermal debinding took 33 h. Finally, the sintering operation was performed at 1400 °C and took 22 h. The exact ramps and other debinding and sintering parameters are not mentioned since it is the know-how of the company which produced the pellets.

### 2.6. Part Characterization

After each of the experimental steps (printing, finish milling and debinding–sintering), the parts were characterized using the same measuring tools: a Keyence VR-6000 profilometer (Keyence, Osaka, Japan) and a Wenzel LH-54 coordinate measuring machine (CMM) (Wenzel Group GmbH & Co. KG, Wiesthal, Germany). The first machine was used to characterize the surface texture of the parts, while the second allowed the parallelism, perpendicularity, flatness and distances to be evaluated.

The profilometer exhibited a measurement accuracy of  $\pm 2 \mu\text{m}$  for the X and Y axes and  $\pm 4 \mu\text{m}$  for Z axis. It was used with a  $40\times$  magnification objective. For each surface of the parts, after milling and sintering, two directions of measurement were considered: parallel and perpendicular to the cutting tool feed direction, as depicted in Figure 5. Ten parallel lines were used following these directions to evaluate the arithmetic and total roughness (Ra and Rt) profile surface texture parameters. The characterization of the surface texture was completed by the evaluation of areal surface texture parameters such as the arithmetic mean height (Sa) and maximal height (Sz). The sampling lengths were selected according to ISO 4288.

Focused ion beam scanning electron microscope (FIB-SEM) images from a TESCAN Gaia 3 (Tescan, Brno, Czech Republic) were also taken on one part to complete the surfaces' qualitative evaluation. The magnification used was  $100\times$ , while the accelerating voltage was set to 10 kV. An unmilled Vertical surface (V4) was measured as well as a milled surface (V2), both after sintering, to allow us to see the improvement brought by milling.

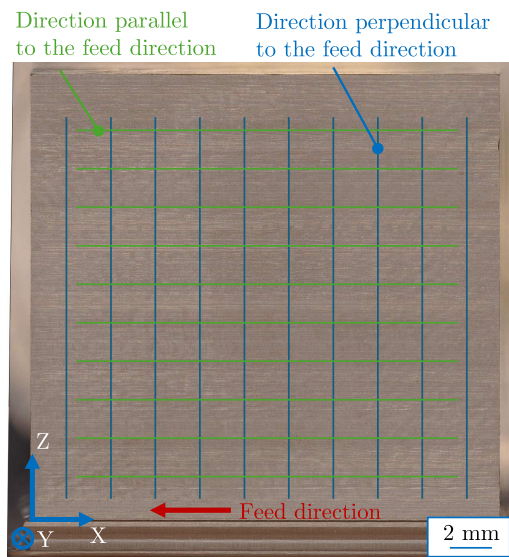


**Figure 5.** Directions of evaluation for the profile surface texture parameters on surface V2; magnification 40 $\times$ .

The CMM uncertainty of measurement (in  $\mu\text{m}$ ) for a given length  $L$  (in mm) was  $3 + L/300$  for the X and Y axes and  $3.5 + L/300$  for the Z axis. This machine was fitted with a spherical probe with a diameter of 5 mm in order to filter the parts' staircase effect generated by the PAM process. The acquisition of data was performed using the Metrosoft QUARTIS measurement software version 2021. All planes were measured by taking 12 randomly distributed points over the entire surface. Evaluation of the distances between Vertical surfaces was conducted, while geometrical characterizations were performed by evaluating the flatness of each surface. The parallelism between the Vertical surfaces and the perpendicularity between Vertical and Top surfaces completed the measurements.

### 3. Results and Discussion

#### 3.1. Qualitative Evaluation

Figure 6 allows a first qualitative evaluation of the parts after the three experimental steps. The Top surface and the Vertical surface V2 are depicted. The as-built parts after step 1 (printing) exhibited a very rough surface texture for their vertical surfaces. This is due to the 0.350 mm layer height, which resulted in a very visible staircase effect. By contrast, the Top surface of the as-built parts was much flatter and more regular, but it was still dull. This is because this surface was in contact with the build platform of the printer during printing. Therefore, the build platform transferred its texture to the surface in contact with it (due to crushing of the first layer).

After step 2 (finish milling), the Vertical and Top surfaces exhibited a shiny and light reflective finish. Nevertheless, the milling tool traces were visible. This is important since it can influence the results of the surface texture. The corners of the parts were also very well defined with very sharp corners thanks to the milling operation.

After step 3 (debinding and sintering), the parts shrank and their sizes were reduced. As can be seen in the picture, the surfaces were still smooth and acquired a black color, which is characteristic of sintered zirconia TZ-black (from Tosoh Corp.). The milling tool traces were still visible and could affect the surface texture. The corners of the parts were still very well defined and sharp.

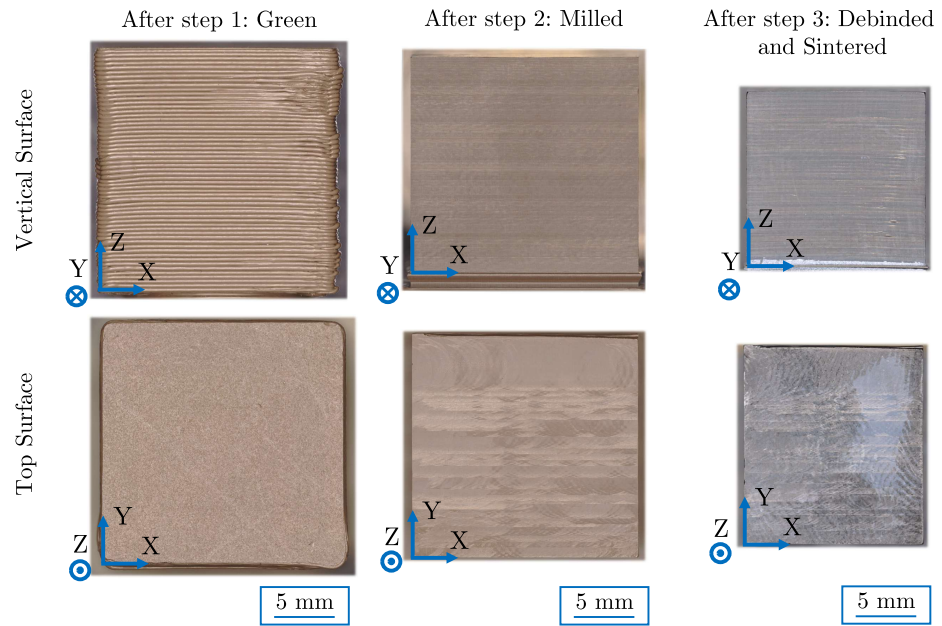


**Figure 6.** Qualitative evaluation of the parts' Vertical (V2) and Top surfaces at the green (as-built after step 1), milled (after step 2) and sintered (after step 3) states; magnification 40×.

A scan of the corner of a part at the green state (after step 1) and after its milling and sintering (after step 3) is given in Figure 7. As can be seen, the corner obtained after sintering was much sharper and better defined compared to the part before milling.

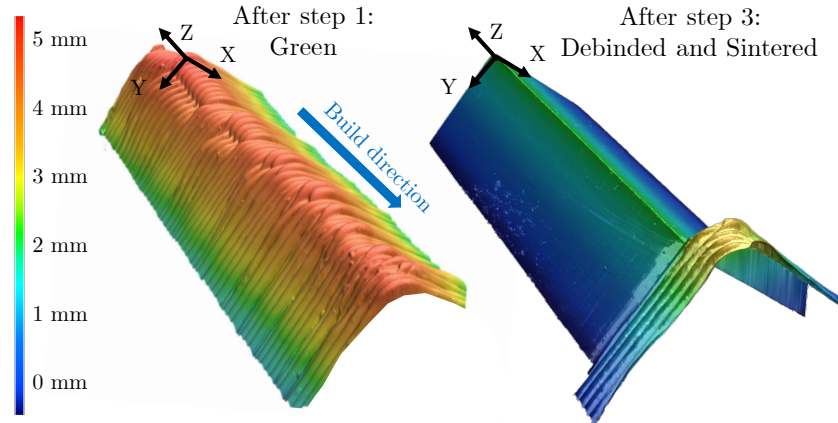


**Figure 7.** Qualitative view of a part's corner at the green state (after step 1) and after the debinding and sintering operations (after step 3); magnification 40×.

Figure 8 depicts the FIB-SEM images of one unmilled Vertical surface (V4, Figure 8a) and one milled Vertical surface (V2, Figure 8b), both after sintering. Both images were taken with a magnification of 100× and an accelerating voltage of 10 kV. The improvement brought by the milling operation prior to sintering can be clearly seen due to the smooth surface. Some small tool traces can still be noticed on the milled surface, while chips are visible between the deposited layers of the unmilled part.

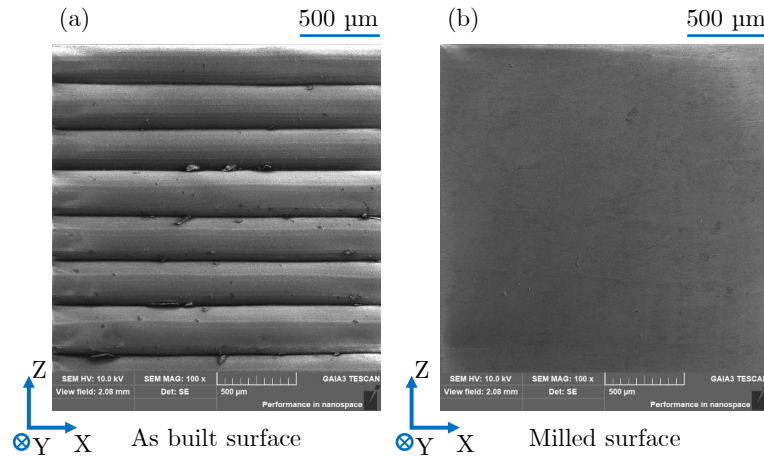


**Figure 8.** FIB-SEM pictures of the unmilled Vertical surface V4 after sintering (a) and the milled Vertical surface V2 after sintering (b); magnification 100×.

3.2. Dimensional Characterization

Figure 9 gives the distances between the Vertical surfaces after each of the steps: each bar representing three measurements with  $\pm \sigma$  error bars. Comparing the distances between V1 and V3 (V1V3) and between V2 and V4 (V2V4), the reduction of size after the milling operation was not the same. Indeed, V4 is the Vertical surface that was not milled in order to act as a witness for comparison after the sintering operation. As a result, V1V3 lost on average 2.668 mm, while V2V4 lost only 1.219 mm. With respect to the performed milling passes (1.5 mm on each Vertical surface), less material than expected was removed. This demonstrates the difficulty of taking references on an AM part in order to mill it. Indeed, milling machines, such as the robotic arm used in this study, require the taking of vectors to locate the part in their workspace. Since the parts exhibited an elephant foot defect, as shown in Figure 10, which is common for AM parts obtained by material extrusion, it was very difficult to achieve accurate positioning of the robotic arm with respect to the part. This explains why the distance reduction was lower than expected. As a consequence, the total material thickness removed from the Vertical surfaces V1 and V3 was 1.334 mm on average instead of 1.500 mm, while 1.219 mm was removed from surface V2. After the sintering operation, V1V3 distance was decreased to 13.790 mm, and the V2V4 distance decreased to 14.832 mm, leading to an average shrink factor of 1.264. This approached the shrink factor announced by the pellet supplier for parts with a wall thickness of 5 mm: 1.280.

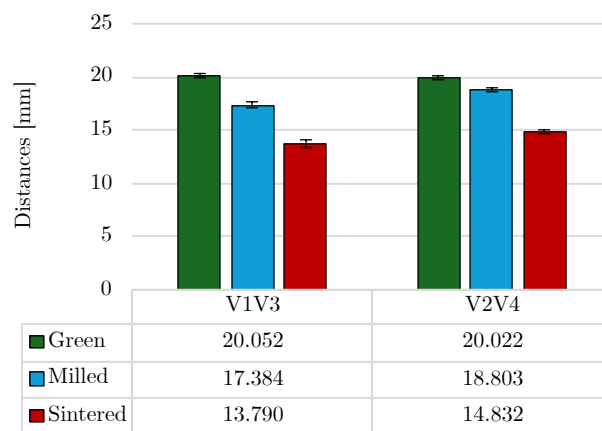


**Figure 9.** Vertical plane distances (in mm) for the green (as-built after step 1), milled (after step 2) and sintered (after step 3) states of the parts.

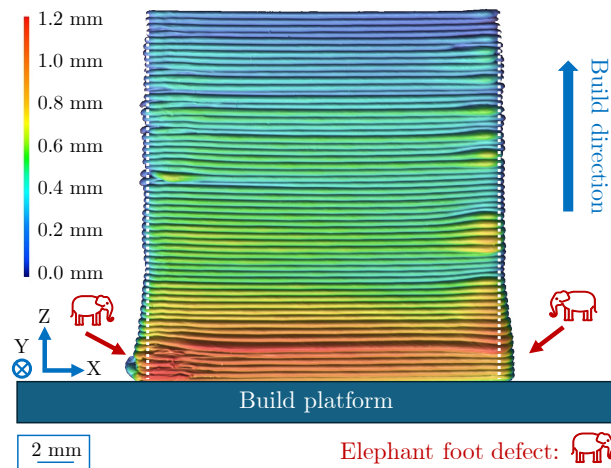


**Figure 10.** Elephant foot defect at the interface between the part and the build platform for surface V2; magnification 40×.

### 3.3. Geometrical Characterization

The measurements of the Vertical and Top surfaces allowed us to also monitor the evolution of several geometrical characteristics. Each bar of the following graphs represents three measurements with  $\pm \sigma$  error bars. Figure 11, for example, gives the flatness of the Top and Vertical surfaces at the three considered stages of the part. As can be seen on the graph, the flatness after step 1 (printing) was very different for the Top and Vertical surfaces, with average values of 0.060 mm and 0.308 mm, respectively. This difference comes from the position given to the parts during their printing, as highlighted in the qualitative evaluation. Indeed, the Top surface was in contact with the build platform, while the Vertical surfaces were aligned with the build direction. As a consequence, the Top surface mostly acquired the surface texture of the build platform, while the Vertical surfaces were affected by the selected layer height and the resulting staircase effect.

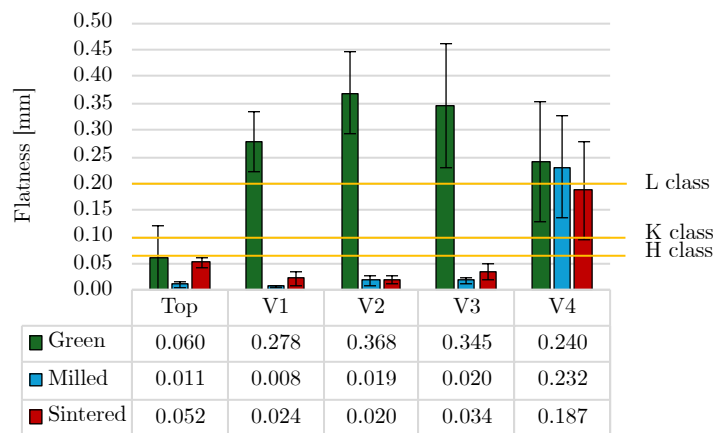


**Figure 11.** Flatness deviation (in mm) of the Top and Vertical surfaces (V1 to V4) for the green (after step 1), milled (after step 2) and sintered (after step 3) states of the parts.

After step 2 (milling operation), all the results were within the same order of magnitude, with values below 0.020 mm for all Top and Vertical surfaces, except V4, which was not milled. The flatness deviation of the surfaces was divided by about 15. This significant improvement allowed the milled Vertical surfaces to improve from an ISO 2768-2 L (large) class to an H (fine) class. Moreover, the absolute value of the standard deviations was significantly decreased. With respect to the mean value, it was still in the same order of magnitude, with variations between the parts reaching, on average, 38% of the mean value.

Nevertheless, although the milling process did not improve the disparities between the three milled parts, it did not degrade them either.

Step 3 (sintering operation) had a direct influence on the flatness results. Indeed, for the Vertical surfaces V1, V2 and V3, it almost doubled, on average, the flatness deviation. However, the flatness of these surfaces still belonged to the H (fine) class of ISO 2768-2 after sintering. Even if the sintering negatively affected the flatness of the parts, compared to the green parts, the sintered ones exhibited an improvement in flatness by a factor of 13.3 on average. For the Top surface, the results were worse, with nearly five times higher flatness after sintering with respect to the flatness after milling. This is due to the position of the parts during this operation: they were laid on the Top surface to withstand the debinding and sintering operations. Moreover, the sharp edges created by the milling operation at the corner of the parts could also affect the sintering process, leading to temperature gradients and residual stresses. These reasons may explain the poorer flatness of the Top surface. However, even if the results were worse than before, the average flatness of the Top surface still belonged to the H (fine) class of ISO 2768-2 after sintering. Therefore, the flatness was affected by the sintering operation but not significantly with respect to the ISO 2768-2 classes. When it comes to the V4 surface, it allowed use to evaluate what would have been the flatness of the parts after sintering if they were not milled. The sintering operation resulted in slightly better flatness: 0.187 mm instead of 0.240 mm on average. However, although sintering decreased the flatness of V4 by a factor 1.3, it still belonged to the ISO 2768-2 L (large) class, while the other Vertical surfaces reached the H (fine) class. The dispersion of the measurements between the parts was neither improved nor worsened due to the sintering operation: it was still within the same order of magnitude and was very large.

The same degradation due to the sintering operation (step 3) was obtained for the parallelism of the V1 and V3 surfaces, as depicted in Figure 12. Indeed, at the green state (after step 1), the parts exhibited a parallelism deviation of about 0.674 mm with a very large standard deviation ( $\pm 0.309$  mm). With respect to ISO 2768-2, this deviation of parallelism belongs to the L (large) class. After milling, the surfaces were improved significantly, leading to parallelism reaching 0.023 mm (improvement by a factor 29.3) and the ISO 2768-2 H (fine) class. Again, the sintering operation degraded the parallelism and nearly doubled it. However, even with this increase, it is still within the H (fine) class (0.060 mm is the class limit, while the parallelism reached 0.037 mm). Nevertheless, compared to the parts before milling, the sintered parts exhibited an 18-times lower parallelism deviation.

The perpendicularity of the part surfaces was also evaluated after each manufacturing step, as shown in Figure 13. Again, the same conclusions can be drawn: the sintering operation (step 3) had a negative impact on the perpendicularity deviation. However, as for the flatness and parallelism, the improvement obtained by milling in terms of the ISO 2768-2 class remained after sintering. Indeed, all results belonged to the K (medium) class at the green stage (step 1) and were lowered to the H (fine) class after milling (step 2). The sintering operation, again, increased the perpendicularity deviation by a factor of about 2.47. However, the sintered parts still exhibited, on average, a decrease by a factor of 8.65 compared to the green parts. On the contrary, the relative standard deviation, on average, was neither decreased nor increased.

Finally, the geometrical characterization was completed by measurement of the corners between the parts' Vertical surfaces. Figure 14 gives the angles between the Vertical surfaces of the parts. As can be seen, the green parts (after step 1) already exhibited an angle between their Vertical surfaces that complied with the target ( $90.435^\circ$ ). However, the measurement dispersion was high, with values of  $\pm 2.2^\circ$ . The milling operation (step 2) allowed this dispersion to be reduced to  $\pm 0.3^\circ$  while improving the angle by better approaching the  $90^\circ$  target ( $90.068^\circ$  on average). After sintering (step 3), the mean value of the angle was slightly increased to  $90.256^\circ$ , while the measurement dispersion maintained  $\pm 0.3^\circ$ . Therefore, even if the sintering operation slightly increased the angle between the Vertical surfaces, it kept the uniformity of the results.

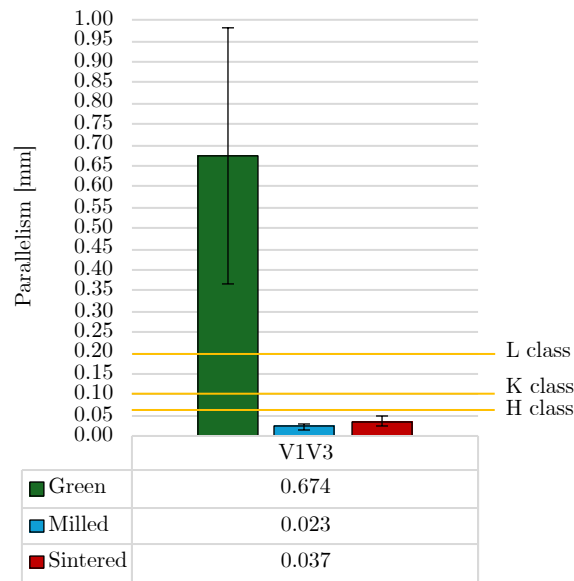


**Figure 12.** Parallelism deviation (in mm) between the V1 and V3 Vertical surfaces for the green (after step 1), milled (after step 2) and sintered (after step 3) states of the parts.

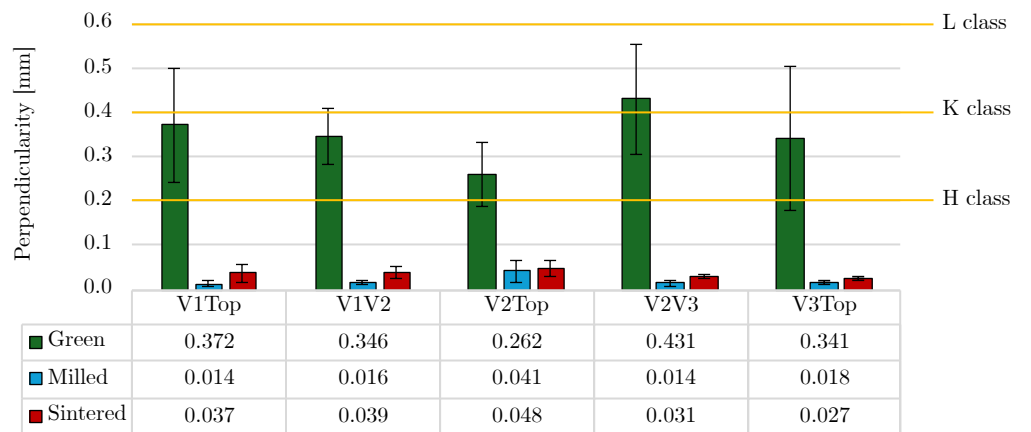


**Figure 13.** Perpendicularity deviation (in mm) of the part Top and Vertical surfaces for the green (after step 1), milled (after step 2) and sintered (after step 3) states of the parts.

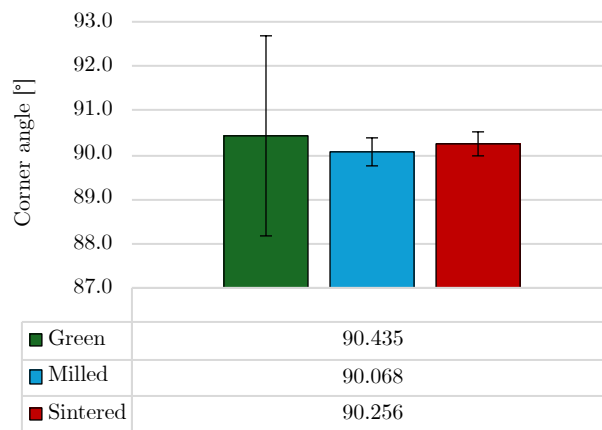


**Figure 14.** Corner angle (in degrees) between the Vertical surfaces of the parts for the green (after step 1), milled (after step 2) and sintered (after step 3) states.

Finally, the corner radii between the parts' Vertical surfaces are given in Figure 15. In this case, the milling operation (step 2) showed very high improvement to the corners by decreasing their radii by 95% compared to the parts' green state (after step 1). The obtained corners were much sharper. The measurement dispersion was also improved from  $\pm 0.112$  mm to  $\pm 0.010$  mm. The sintering operation again improved the results and allowed radii of  $0.037$  mm  $\pm 0.003$  mm to be obtained. These sharp edges would not have been possible to be achieved by the printer without the milling step. Indeed, the minimum radius of curvature that can be generated using an MEX printer is equivalent to the radius of the selected nozzle [36]. Therefore, the theoretical minimum radius that could be achieved by the printer in the selected configuration is 0.500 mm.

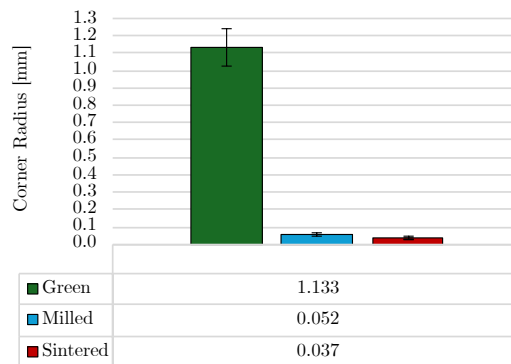


**Figure 15.** Corner radii (in mm) between the Vertical surfaces of the parts for the green (after step 1), milled (after step 2) and sintered (after step 3) states.

### 3.4. Surface Texture Evaluation

The finish milling operation aimed to not only improve the geometry of the parts but also their surface texture. Table 2 shows the Ra, Rt, Sa and Sz measurements on the Top and Vertical surfaces at the green state (step 1) before finish milling. Except for the Top surface, the surface textures after printing were very poor, with the Ra reaching 45.8  $\mu$ m and an Rt of about 280.4  $\mu$ m. This was expected, since the Vertical surfaces were printed along the build direction and, therefore, suffered from the staircase effect due to the high selected layer thickness (0.350 mm). By contrast, the Top surface exhibited better results, with an Ra of 2.2  $\mu$ m and an Rt of 2.5  $\mu$ m. Indeed, as explained for the flatness deviation, this surface was in contact with the printer's build platform. Therefore, the Top surface acquired the build platform's very flat and smooth texture. However, although the Rt was good, the Sz was higher: on average, 106.9  $\mu$ m. The same behavior is exhibited by the Vertical surfaces, with Sz values of 962.5  $\mu$ m, while the Rt reached 280.4  $\mu$ m. This can be explained by the flatness deviation due to the printing process itself. Indeed, even though fillets were added in the part design, small warping occurred at the part corners, leading to worse flatness of the Top surface. Moreover, the elephant foot defect that was already mentioned in the flatness evaluation also played a role in the very high values of Sz for the Vertical surfaces. All these defects again motivated the use of milling to improve the surface geometry and texture.

**Table 2.** Profile (Ra and Rt) and areal (Sa and Sz) surface texture parameters for the Top and Vertical surfaces of the part at the green state.

	Top	Vertical
Ra [ $\mu$ m]	2.2 $\pm$ 1.4	45.8 $\pm$ 6.8
Rt [ $\mu$ m]	16.4 $\pm$ 10.8	280.4 $\pm$ 40.5
Sa [ $\mu$ m]	2.5 $\pm$ 2	67.3 $\pm$ 9.5
Sz [ $\mu$ m]	106.9 $\pm$ 25.9	962.5 $\pm$ 208.6

Figure 16 gives the obtained arithmetic roughness (Ra) measurements after the milling (step 2) and sintering (step 3) steps. Each bar in the following graphs represents 30 measurements with  $\pm \sigma$  error bars. Indeed, as shown in Figure 5, the profile surface texture parameters were evaluated across 10 parallel lines on each of the three parts. The graph is divided into two main directions: along the feed of the milling operations (Feed) and perpendicular to this direction (Perp.). This allows us to see the influence of the overlap between the milling passes. Indeed, both for the Top and Vertical surfaces, the Ra results were significantly different across these two directions, with almost one Ra class of difference. In the case of the Vertical surfaces, no overlap was performed during the milling operation. This may explain the difference between the results along feed direction and perpendicular to it. For the Top surface, an overlap of about 10% was obtained. However, a difference was still observed. In this case, the overlap allowed the standard deviation to be decreased with respect to the Vertical surfaces. Moreover, the tool is composed of different geometries for its end and side teeth. They then generated different levels of Ra. Therefore, this explains why the Top surface exhibited a slightly better surface texture. Even with the difference in both directions, the sintering operation did not significantly influence the Ra results except for the Top surface in the feed direction, which underwent an increase and a class change from Ra < 0.4  $\mu\text{m}$  to Ra < 0.8  $\mu\text{m}$  after sintering.

However, the decrease in Ra for all surfaces brought by the milling operation (step 2), which was mostly preserved by the sintering operation (step 3), was significant. It provided an improvement of 5 Ra classes for the Vertical surfaces (from Ra < 50  $\mu\text{m}$  to Ra < 1.6  $\mu\text{m}$ ) and an improvement of 1 Ra class for the Top surface (from Ra < 3.2  $\mu\text{m}$  to Ra < 1.6  $\mu\text{m}$ ). Moreover, Ra < 1.6  $\mu\text{m}$  was obtained for all surfaces after sintering, demonstrating the advantage of conducting finishing operations on AM printed parts.

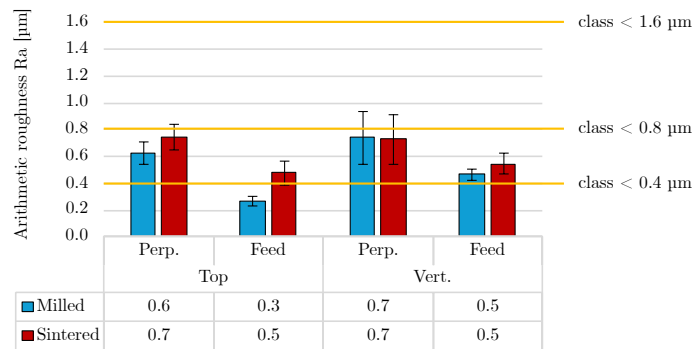
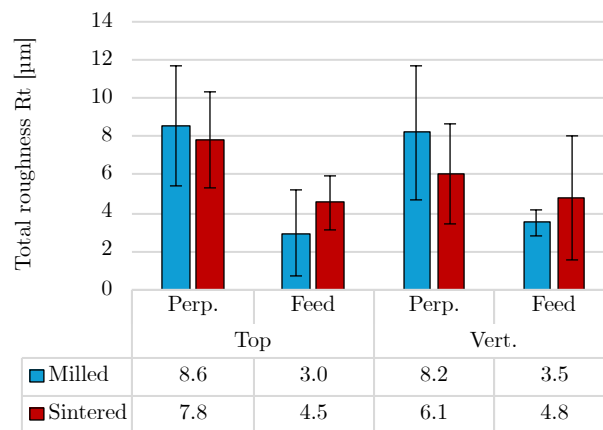


Figure 16. Arithmetic roughness (Ra in  $\mu\text{m}$ ) of the parts’ Top and Vertical surfaces for the milled (after step 2) and sintered (after step 3) states; “Perp.” stands for the direction perpendicular to the feed (“Feed”) direction.

The same observations can be made in Figure 17, which shows the results for the Rt across the feed direction and perpendicular to it for the Top and Vertical surfaces. Indeed, the results across the feed direction and perpendicular to it were different, showing the influence of the absence of overlap for the Vertical surfaces. Again, the sintering operation (step 3) did not significantly change the Rt results except for the Top surfaces, for which it increased them slightly while reducing the dispersion of results between the parts. As before, the position of the part during the debinding and sintering operation can influence the surface texture and may explain this tendency. Nevertheless, the Rt results after sintering (step 3) were still very good and were significantly lower compared to those of the as-built parts (step 1). Indeed, they decreased by one and two orders of magnitude for the Top and Vertical surfaces, respectively.

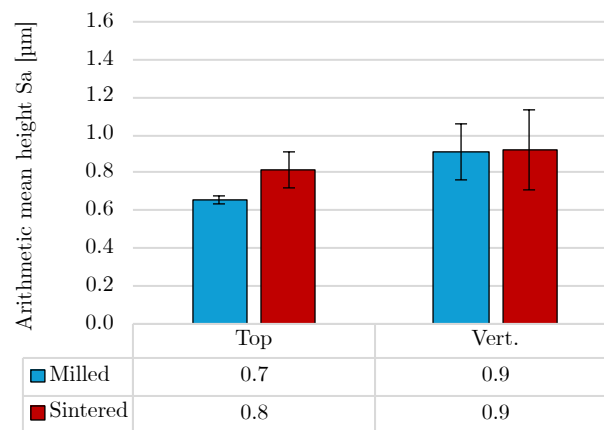


**Figure 17.** Total roughness (Rt in  $\mu\text{m}$ ) of the parts’ Top and Vertical surfaces for the milled (after step 2) and sintered (after step 3) states: “Perp.” stands for the direction perpendicular to the feed (“Feed”) direction.

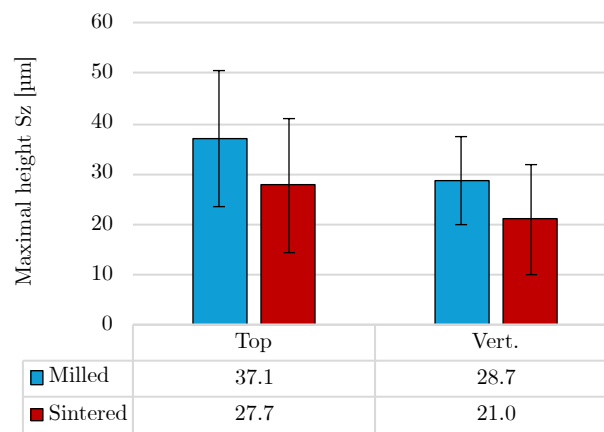
Even though Ra and Rt are among the most widespread indicators of surface texture across the industry in recent years, they are influenced by the position of the probe within the milling tool traces on the surface to be measured [38]. Moreover, since the profile is unidirectional, these measurement techniques cannot provide information about the exact nature of a topographic feature, e.g., if a sudden drop in the recorded profile is a pit or a valley, for example [39]. Precautions should then be taken while using profile measurements. Therefore, the use of areal surface texture parameters (Sa and Sz, for example) is becoming more widespread because they allow researchers to encompass three directions instead of two and have more statistical significance [39].

Figure 18 gives the Sa results: each bar represents three measurements with  $\pm\sigma$  error bars. In this case, no distinction was made between the feed direction and perpendicular to it since the parameters are areal. As with the Ra, the measurements were all below the  $1.6\ \mu\text{m}$  threshold. Some slight differences can be seen for the Top surface after milling (step 2), which reached results below  $0.8\ \mu\text{m}$ . Again, this difference was expected since this surface was obtained by an end milling operation, while the Vertical surfaces were obtained by side milling. The sintering operation (step 3) seemed to have no effect on the Sa results of the Vertical surfaces. Indeed, the measurements after sintering were the same as after milling, with slight changes in measurement dispersion. This was not the case for the Top surface, which degraded slightly and achieved measurements higher than  $0.8\ \mu\text{m}$  for some parts. As before, this slight degradation may come from the position of the part during the debinding and sintering operations. However, the Sa measurements were still very good. Again, the improvement in terms of Sa after the sintering operation with respect to the as-built parts is significant, with reductions by a factor about 75 for the Vertical surfaces and about 3 for the Top surface.

Figure 19 shows the Sz results for the Top and Vertical surfaces. The results were higher than those for Rt and also had a higher relative measurement dispersion. This shows the importance of the areal surface texture parameters since they allow researchers to provide a measurement across the entire surface. Again, the influence of the milling mode can be seen, with different measurements after milling for the Top and Vertical surfaces. After the sintering operation, the Sz results decreased slightly, while the measurement dispersion increased between the parts. The improvement with respect to the as-built parts was also significant, with reductions by a factor about 46 for the Vertical surfaces and about 8 for the Top surface.



**Figure 18.** Arithmetic mean height ( $S_a$  in  $\mu\text{m}$ ) of the parts' Top and Vertical surfaces for the milled (after step 2) and sintered (after step 3) states.



**Figure 19.** Maximum height ( $S_z$  in  $\mu\text{m}$ ) of the parts' Top and Vertical surfaces for the milled (after step 2) and sintered (after step 3) states.

#### 4. Future Prospects

In this paper, a finish milling process was applied to ceramic green parts to enhance their surface textures and geometrical tolerances. However, other non-conventional techniques such as laser processing can offer additional possibilities for the produced parts depending on their final applications. For example, SiC (silicon carbide) ceramics are used in a wide range of applications where tribological properties are of prime interest: bearings, piston ring/cylinder liners for combustion engines, or mechanical seals, for example [40]. Parts made from this material could be enhanced by using laser processing to obtain artificial micro-dimples or micro-grooves to work as lubricant reserves. Another area where tribological properties must be controlled is the biomedical sector. Indeed, bioinert ceramics such as zirconia and alumina are widely used to manufacture implants [41]. For example, orthopedic implants for total hip arthroplasty can be manufactured using composites made of zirconia and alumina and called alumina-toughened zirconia (ATZ) ceramics [42]. This kind of implant requires excellent friction behavior to reduce wear between the moving parts and to ensure reliable implant operation [43].

Furthermore, the surface texture also plays a critical role in the osseointegration process for implants and enhances soft tissue attachment [44]. Again, laser processing is attractive in this case since it allows the generation of hierarchical surface textures without the risk of contamination (contact-free treatment) while controlling the wettability of the surfaces of materials regardless of their mechanical properties and hardness. This was recently tested on a pre-sintered alumina zirconia composite by Bains et al. [45] and led

to the fabrication of real acetabular cups for hip joint prosthesis. The surface texture of the parts was in the same range as the osteoblastic cell sizes and should therefore promote growth and interlocking of the bone tissue within the cup. Other examples can be found in the recent review by De Zanet et al. [46].

Laser processing can also be performed on green parts [47]. This reduces the risk of micro-cracks and avoids potential modification of the microstructure of the surface due to laser-induced thermal loads [48]. The time to manufacture micro-features is lower in the case of laser processing compared to conventional micro-milling, and this process can generate sharper edges and does not require firm attachment [47]. Therefore, a hybrid machine composed of a PAM extruder and a spindle could be completed by a pulsating laser. This is a direct perspective for this work and would allow the produced parts to have improved tribological properties, fine aesthetic features or new functions (for example, osseointegration).

Even if hybrid manufacturing allows manufacturers to decrease the material waste compared to conventional subtractive processes as milling, it still generates chips. However, this waste can be reused and inserted into the PAM extruder [49,50]. Many studies have been conducted to test the feasibility of recycling the conventional polymers used in MEX: mainly, PLA and ABS [7]. However, recycling the chips of thermoplastic ceramic composites such as the one used in this paper has not been covered in the literature. This could be another interesting perspective for this work. Recycling of conventional polymers using AM progressively decreases the mechanical properties of the generated parts [51]. However, for the sake of thermoplastic ceramic composites, the polymer is only used as a binder. It is removed when debinding and sintering the part. Therefore, a decrease in mechanical properties should not be a problem in this case.

## 5. Conclusions

The proposed study focused on the manufacturing of composite zirconia parts using a hybrid approach combining PAM with ceramic injection molding feedstock and milling. It is the first study to quantify the improvements in surface texture and geometrical tolerances achieved by a finish milling operation on PAM-shaped composite green parts. The influence of the debinding and sintering processes on these characteristics was assessed as well as the overall improvements that were achieved with respect to the initial composite green parts. This paper contributed to a better understanding of the surface textures and geometrical tolerances that can be obtained using a hybrid approach.

These are the main conclusions of the paper:

- From a qualitative point of view, the finish milling operation allowed shiny and smooth surfaces to be obtained, while sharp edges that are impossible to obtain by PAM were generated. Debinding and sintering did not affect these characteristics.
- The debinding and sintering operations shrank the part in the X and Y directions by a factor 1.264 on average, while the supplier announced shrinkage of 1.280.
- The milling operation allowed the flatness, parallelism and perpendicularity deviations of the part's surfaces to be improved. The H (fine) class of ISO 2768-2 was achieved thanks to this operation, while the green parts before milling mostly exhibited an L (large) class. However, the debinding and sintering operations had a significant influence on these characteristics and increased their average by a factor of up to five. Nevertheless, the sintered parts still belonged to the H (fine) class and exhibited between 8 and 18 times lower deviations than the green parts.
- The repeatability of the angles between the vertical surfaces was improved by the milling operation, while the corner radii were dramatically decreased by 95%. After sintering, the angles between the vertical surfaces remained stable, while the corner radii decreased again and reached, on average, 0.037 mm. A significant improvement from poorly defined corners to very sharp edges was obtained thanks to the finish milling and the debinding/sintering operations.

- The finish milling operation decreased the Ra of the Vertical surfaces by 5 classes and allowed values below 1.6  $\mu\text{m}$  to be achieved. The sintering operation neither degraded nor improved these results. The Rt, Sa and Sz parameters followed the same trend, with significant improvement brought by the milling operation and no significant change to the results due to the sintering process.

**Author Contributions:** Conceptualization, F.D., E.R.-L., L.S., P.-J.A., F.P., V.D., J.B., C.D., G.M., E.J., R.C. and A.B.O.; methodology, L.S., A.B.O., J.B., C.D., G.M., F.P., E.J. and R.C.; software, L.S.; validation, F.D., E.R.-L., V.D., J.B., C.D., G.M., F.P., E.J., R.C. and L.S.; formal analysis, L.S.; investigation, L.S. and A.B.O.; resources, F.P., F.D. and E.R.-L.; data curation, L.S.; writing—original draft preparation, L.S.; writing—review and editing, F.D., E.R.-L., P.-J.A., F.P., V.D., J.B., C.D., G.M., E.J., R.C. and L.S.; visualization, L.S.; supervision, F.D., E.R.-L., F.P. and P.J.A.; project administration, L.S., F.D., E.R.-L., F.P. and P.-J.A.; funding acquisition, F.P., F.D. and E.R.-L. All authors have read and agreed to the published version of the manuscript.

**Funding:** The Walloon regional government funded this research under grant 2110084 (HyProPAM research project).

**Data Availability Statement:** The data presented in this study are available on request from the corresponding author.

**Conflicts of Interest:** The authors declare no conflicts of interest.

## References

- Galusek, D.; Ghillányová, K. Ceramic Oxides. In *Ceramics Science and Technology*; Riedel, R., Chen, I.W., Eds.; Wiley-VCH Verlag GmbH & Co. KGaA: Weinheim, Germany, 2014; pp. 1–58. <https://doi.org/10.1002/9783527631940.ch13>.
- Altıparmak, S.C.; Yardley, V.A.; Shi, Z.; Lin, J. Extrusion-based additive manufacturing technologies: State of the art and future perspectives. *J. Manuf. Process.* **2022**, *83*, 607–636. <https://doi.org/10.1016/j.jmapro.2022.09.032>.
- Ferraris, E.; Vleugels, J.; Guo, Y.; Bourell, D.; Kruth, J.P.; Lauwers, B. Shaping of engineering ceramics by electro, chemical and physical processes. *CIRP Ann. Manuf. Technol.* **2016**, *65*, 761–784. <https://doi.org/10.1016/j.cirp.2016.06.001>.
- Thompson, M.K.; Moroni, G.; Vaneker, T.; Fadel, G.; Campbell, R.I.; Gibson, I.; Bernard, A.; Schulz, J.; Graf, P.; Ahuja, B.; et al. Design for Additive Manufacturing: Trends, opportunities, considerations, and constraints. *CIRP Ann. Manuf. Technol.* **2016**, *65*, 737–760. Publisher: CIRP, <https://doi.org/10.1016/j.cirp.2016.05.004>.
- Gupta, S. Zirconia for Dental Implants. In *Additive Manufacturing in Biomedical Applications*; Narayan, R.J., Ed.; ASM International: Cleveland, OH, USA, 2022; pp. 479–485. <https://doi.org/10.31399/asm.hb.v23A.a0006853>.
- Gonzalez-Gutierrez, J.; Cano, S.; Schuschnigg, S.; Kukla, C.; Sapkota, J.; Holzer, C. Additive Manufacturing of Metallic and Ceramic Components by the Material Extrusion of Highly-Filled Polymers: A Review and Future Perspectives. *Materials* **2018**, *11*, 840. <https://doi.org/10.3390/ma11050840>.
- Paxton, N.C.; Zhao, J.; Sauret, E. Polymer 3D printing in perspective: Assessing challenges and opportunities in industrial translation against the metal benchmark. *Int. J. Adv. Manuf. Technol.* **2024**, *133*, 59–80. <https://doi.org/10.1007/s00170-024-13744-z>.
- Mobarak, M.H.; Islam, M.A.; Hossain, N.; Al Mahmud, M.Z.; Rayhan, M.T.; Nishi, N.J.; Chowdhury, M.A. Recent advances of additive manufacturing in implant fabrication—A review. *Appl. Surf. Sci. Adv.* **2023**, *18*, 100462. <https://doi.org/10.1016/j.apsadv.2023.100462>.
- ISO/ASTM 52900:2021; Additive Manufacturing General Principles Fundamentals and Vocabulary. Geneva, Switzerland, 2021.
- Smartechnology Analysis Ceramics Additive Manufacturing Markets 2017–2028, an Opportunity Analysis and Ten-Year Market Forecast. Technical Report; Dublin, Ireland, 2018. Available online: <https://additivemanufacturingresearch.com/reports/ceramics-additive-manufacturing-markets-2017-2028/> (accessed on June the 21st)
- Lakhdar, Y.; Tuck, C.; Binner, J.; Terry, A.; Goodridge, R. Additive manufacturing of advanced ceramic materials. *Prog. Mater. Sci.* **2021**, *116*, 100736. <https://doi.org/10.1016/j.pmatsci.2020.100736>.
- Guerra, M.G.; Morfini, L.; Pellegrini, A.; Meng, F.; Lavecchia, F.; Ferraris, E.; Galantucci, L.M. Material Extrusion-Debinding-Sintering as an Emerging Additive Manufacturing Process Chain for Metal/Ceramic Parts Construction. In *CIRP Novel Topics in Production Engineering*; Tolio, T., Ed.; Springer Nature Switzerland: Cham, Switzerland, 2024; Volume 1, pp. 147–182. [https://doi.org/10.1007/978-3-031-54034-9\\_5](https://doi.org/10.1007/978-3-031-54034-9_5).
- Li, W.; Leu, M.C. Material Extrusion Based Ceramic Additive Manufacturing. In *Additive Manufacturing Processes*; Bourell, D.L., Frazier, W., Kuhn, H., Seifi, M., Eds.; ASM International: Cleveland, OH, USA, 2020; pp. 97–111. <https://doi.org/10.31399/asm.hb.v24.a0006562>.
- Prawel, D.A. Material Extrusion Additive Manufacturing Systems. In *ASM Handbook—Additive Manufacturing Processes*; ASM International: Cleveland, OH, USA, 2020; Volume 24. <https://doi.org/10.31399/asm.hb.v24.a0006580>.
- Rane, K.; Strano, M. A comprehensive review of extrusion-based additive manufacturing processes for rapid production of metallic and ceramic parts. *Adv. Manuf.* **2019**, *7*, 155–173. <https://doi.org/10.1007/s40436-019-00253-6>.

16. Moïnard, D.; Rigollet, C. Procédés de frittage PIM. *Tech. L'Ingénieur* **2011**, TIB633DUO.
17. Patti, A. Challenges to Improve Extrusion-based Additive Manufacturing Process of Thermoplastics Towards Sustainable Development. *Macromol. Rapid Commun.* **2024**, 2400249. <https://doi.org/10.1002/marc.202400249>.
18. He, Q.; Jiang, J.; Yang, X.; Zhang, L.; Zhou, Z.; Zhong, Y.; Shen, Z. Additive manufacturing of dense zirconia ceramics by fused deposition modeling via screw extrusion. *J. Eur. Ceram. Soc.* **2021**, *41*, 1033–1040. <https://doi.org/10.1016/j.jeurceramsoc.2020.09.018>.
19. Rane, K.; Farid, M.A.; Hassan, W.; Strano, M. Effect of printing parameters on mechanical properties of extrusion-based additively manufactured ceramic parts. *Ceram. Int.* **2021**, *47*, 12189–12198. <https://doi.org/10.1016/j.ceramint.2021.01.066>.
20. Gibson, I.; Rosen, D.; Stucker, B.; Khorasani, M. *Additive Manufacturing Technologies*; Springer International Publishing: Cham, Switzerland, 2021. <https://doi.org/10.1007/978-3-030-56127-7>.
21. Golhin, A.P.; Tonello, R.; Frisvad, J.R.; Grammatikos, S.; Strandlie, A. Surface roughness of as-printed polymers: A comprehensive review. *Int. J. Adv. Manuf. Technol.* **2023**, *127*, 987–1043. <https://doi.org/10.1007/s00170-023-11566-z>.
22. Kellens, K.; Mertens, R.; Paraskevas, D.; Dewulf, W.; Dufloy, J.R. Environmental Impact of Additive Manufacturing Processes: Does AM Contribute to a More Sustainable Way of Part Manufacturing? *Procedia CIRP* **2017**, *61*, 582–587. <https://doi.org/10.1016/j.procir.2016.11.153>.
23. Kara, S.; Li, W. Unit process energy consumption models for material removal processes. *CIRP Ann.* **2011**, *60*, 37–40. <https://doi.org/10.1016/j.cirp.2011.03.018>.
24. Boulanger, J. Tolérances et écarts dimensionnels, géométriques et d'états de surface. *Tech. L'Ingénieur, Travail des matériaux - Assemblage* **1991**, b7010. <https://doi.org/10.51257/a-v1-b7010>.
25. Demarbaix, A.; Mulliez, M.; Rivière-Lorphèvre, E.; Spitaels, L.; Duterte, C.; Preux, N.; Petit, F.; Ducobu, F. Green Ceramic Machining: Determination of the Recommended Feed Rate for Y-TZP Milling. *J. Compos. Sci.* **2021**, *5*, 231. <https://doi.org/10.3390/jcs5090231>.
26. Parenti, P.; Cazzani, A.; Annoni, M. Cutting force modelling in green machining of polymer-based metallic feedstock. *J. Mater. Process. Technol.* **2023**, *312*, 117825. <https://doi.org/10.1016/j.jmatprotec.2022.117825>.
27. Spitaels, L.; Dantinne, H.; Bossu, J.; Rivière-Lorphèvre, E.; Ducobu, F. A Systematic Approach to Determine the Cutting Parameters of AM Green Zirconia in Finish Milling. *J. Compos. Sci.* **2023**, *7*, 112. <https://doi.org/10.3390/jcs7030112>.
28. Flynn, J.M.; Shokrani, A.; Newman, S.T.; Dhokia, V. Hybrid additive and subtractive machine tools – Research and industrial developments. *Int. J. Mach. Tools Manuf.* **2016**, *101*, 79–101. <https://doi.org/10.1016/j.ijmactools.2015.11.007>.
29. Grzesik, W.; Ruszaj, A. *Hybrid Manufacturing Processes: Physical Fundamentals, Modelling and Rational Applications*; Springer Series in Advanced Manufacturing; Springer International Publishing: Cham, Switzerland, 2021. <https://doi.org/10.1007/978-3-030-77107-2>.
30. Hafenecker, J.; Bartels, D.; Kuball, C.M.; Krefß, M.; Rothfelder, R.; Schmidt, M.; Merklein, M. Hybrid process chains combining metal additive manufacturing and forming—A review. *CIRP J. Manuf. Sci. Technol.* **2023**, *46*, 98–115. <https://doi.org/10.1016/j.cirpj.2023.08.002>.
31. ISO 286-1:1988; Geometrical Product Specifications (GPS)—ISO System of Limits and Fits—Part 1: Bases of Tolerances, Deviations and Fits. ISO: Geneva, Switzerland, 1988.
32. ISO 2768-1:1989; General Tolerances—Part 1: Tolerances for Linear and Angular Dimensions without Individual Tolerance Indications. ISO: Geneva, Switzerland, 1989.
33. ISO 2768-2:1989; General Tolerances—Part 2: Geometrical Tolerances for Features without Individual Tolerance Indications. ISO: Geneva, Switzerland, 1989.
34. ISO 4288:1996; Geometrical Product Specifications (GPS)—Surface Texture: Profile Method Rules and Procedures for the Assessment of Surface Texture. ISO: Geneva, Switzerland, 1996.
35. ISO 17296-3:2014; Additive Manufacturing—General Principles—Part 3: Main Characteristics and Corresponding Test Methods. ISO: Geneva, Switzerland, 2014.
36. Pei, E.; Rosen, D.W.; Seepersad, C. Design Rules. In *Additive Manufacturing Design and Applications*; Seifi, M., Bourell, D.L., Frazier, W., Kuhn, H., Eds.; ASM International: Cleveland, OH, USA, 2023; pp. 97–115. <https://doi.org/10.31399/asm.hb.v24A.a0006948>.
37. Spitaels, L.; Olabarri, N.A.; Bossu, J.; Martic, G.; Juste, E.; Arrazola, P.J.; Rivière-Lorphèvre, É.; Ducobu, F. Tool wear for finishing milling of green thermoplastic-ceramic composites fabricated with pellet AM. *Procedia CIRP* **2024**, *121*, 97–102. <https://doi.org/10.1016/j.procir.2023.09.235>.
38. Todhunter, L.; Leach, R.; Lawes, S.; Blateyron, F. Industrial survey of ISO surface texture parameters. *CIRP J. Manuf. Sci. Technol.* **2017**, *19*, 84–92. <https://doi.org/10.1016/j.cirpj.2017.06.001>.
39. Leach, R. (Ed.) *Characterisation of Areal Surface Texture*; Springer: Berlin/Heidelberg, Germany, 2013. <https://doi.org/10.1007/978-3-642-36458-7>.
40. Zhang, W. Tribology of SiC ceramics under lubrication: Features, developments, and perspectives. *Curr. Opin. Solid State Mater. Sci.* **2022**, *26*, 101000. <https://doi.org/10.1016/j.cossms.2022.101000>.
41. Barnes, D.; Moavenian, A.; Sharma, A.; Best, S. Biocompatibility of Ceramics. In *Materials for Medical Devices*; Narayan, R.J., Ed.; ASM International: Cleveland, OH, USA, 2012; pp. 128–134. <https://doi.org/10.31399/asm.hb.v23.a0005655>.
42. Antoniac, I.V. (ed.). *Handbook of Bioceramics and Biocomposites*; Springer International Publishing: Cham, Switzerland, 2016. <https://doi.org/10.1007/978-3-319-12460-5>.
43. Ramsden, J.; Allen, D.; Stephenson, D.; Alcock, J.; Peggs, G.; Fuller, G.; Goch, G. The Design and Manufacture of Biomedical Surfaces. *CIRP Ann.* **2007**, *56*, 687–711. <https://doi.org/10.1016/j.cirp.2007.10.001>.

44. Han, J.; Zhang, F.; Van Meerbeek, B.; Vleugels, J.; Braem, A.; Castagne, S. Laser surface texturing of zirconia-based ceramics for dental applications: A review. *Mater. Sci. Eng. C* **2021**, *123*, 112034. <https://doi.org/10.1016/j.msec.2021.112034>.
45. Bairo, F.; Montealegre, M.A.; Minguella-Canela, J.; Vitale-Brovarone, C. Laser Surface Texturing of Alumina/Zirconia Composite Ceramics for Potential Use in Hip Joint Prosthesis. *Coatings* **2019**, *9*, 369. <https://doi.org/10.3390/coatings9060369>.
46. De Zanet, A.; Casalegno, V.; Salvo, M. Laser surface texturing of ceramics and ceramic composite materials—A review. *Ceram. Int.* **2021**, *47*, 7307–7320. <https://doi.org/10.1016/j.ceramint.2020.11.146>.
47. Dadhich, P.; Srivas, P.K.; Mohanty, S.; Dhara, S. Microfabrication of green ceramics: Contact vs. non-contact machining. *J. Eur. Ceram. Soc.* **2015**, *35*, 3909–3916. <https://doi.org/10.1016/j.jeurceramsoc.2015.06.025>.
48. Demarbaix, A.; Ducobu, F.; Juste, E.; Petit, F.; Duterte, C.; Rivière-Lorphèvre, E. Experimental investigation on green ceramic machining with nanosecond laser source. *J. Manuf. Process.* **2021**, *61*, 245–253. <https://doi.org/10.1016/j.jmapro.2020.11.031>.
49. Hasan, M.R.; Davies, I.J.; Pramanik, A.; John, M.; Biswas, W.K. Potential of recycled PLA in 3D printing: A review. *Sustain. Manuf. Serv. Econ.* **2024**, *3*, 100020. <https://doi.org/10.1016/j.smse.2024.100020>.
50. Romani, A.; Perusin, L.; Ciurnelli, M.; Levi, M. Characterization of PLA feedstock after multiple recycling processes for large-format material extrusion additive manufacturing. *Mater. Today Sustain.* **2024**, *25*, 100636. <https://doi.org/10.1016/j.mtsust.2023.100636>.
51. Cruz Sanchez, F.A.; Boudaoud, H.; Hoppe, S.; Camargo, M. Polymer recycling in an open-source additive manufacturing context: Mechanical issues. *Addit. Manuf.* **2017**, *17*, 87–105. <https://doi.org/10.1016/j.addma.2017.05.013>.

**Disclaimer/Publisher’s Note:** The statements, opinions and data contained in all publications are solely those of the individual author(s) and contributor(s) and not of MDPI and/or the editor(s). MDPI and/or the editor(s) disclaim responsibility for any injury to people or property resulting from any ideas, methods, instructions or products referred to in the content.